Coherent imaging of the cone mosaic in the living human eye

Susana Marcos and Rafael Navarro

Instituto de Óptica, Consejo Superior de Investigaciones Científicas, Serrano 121, 28006 Madrid, Spain

Pablo Artal

Laboratorio de Óptica, Universidad de Murcia, Campus del Espinardo, 30071 Murcia, Spain

Received June 26, 1995; revised manuscript received October 30, 1995; accepted November 3, 1995

A new system for the recording of high-resolution images of the cone mosaic in the living human fovea has been developed. The experimental method is inspired by stellar speckle interferometry, used in astronomy to resolve binary stars. Series of short-exposure images of small areas of the fovea are registered under coherent illumination. These images show speckle patterns that have some correlation with the topography of the cone mosaic and retain high-resolution information. Such correlation is better revealed in the power spectrum (square modulus of the Fourier transform). The signal-to-noise ratio is increased, without loss of high frequencies, by averaging the power spectra of a number of such speckle patterns. The average power spectra show, in most of the cases, an elliptical ring (or hexagon), whose mean radius corresponds to the characteristic spatial frequency of the cone mosaic (or the inverse of the mean row-to-row cone spacing) at a given retinal location. Good results are obtained in the five normal observers tested, at various retinal eccentricities, up to 1 visual degree, including the center of the fovea for two eyes. We find a decrease in the spatial frequency of the mosaic with the eccentricity and an important intersubject variability, in agreement with anatomical studies.

1. INTRODUCTION

The retinal mosaic of photoreceptors samples the continuous image of the external scene that is formed on the retina and thus transforms the image into a discrete array of signals that is transmitted to higher stages in the visual processing. Since the photoreceptor spacing and its spatial distribution impose a fundamental limitation in spatial vision, several approaches have been carried out by different investigators to obtain accurate data. The first topographical data were provided by histological studies. In 1935 Oesterberg[1] reported photoreceptor density at different retinal locations in a single human retina. Recently Curcio *et al.*[2] provided a detailed anatomical analysis of the distribution of photoreceptors over the entire human retina, as well as its variability between and within subjects. It has been argued that, owing to possible distortions in the preparation of the tissues, anatomical data could differ from the actual density in living eyes. In addition, in terms of visual performance, it is interesting to convert the photoreceptor spacing measured in millimeters to visual degrees, and for donors' eyes that can be done only on the basis of the parameters of a schematic eye.[3] The variations in the retinal magnification between individuals make the data less comparable. Williams[4] developed a noninvasive psychophysical method to map the cone topography across the living human retina, based on an analysis of the moiré patterns produced by aliasing when interference fringes of spatial frequency beyond the resolution limit are imaged on the foveal cone mosaic. Direct observations of the photoreceptor array through the optical system of the eye have been performed in lower vertebrates,[5,6] but conventional imaging of the cone mosaic in the center of the living human fovea is not possible in most cases, because the optical image quality of the eye is not good enough to resolve the close cone spacing. To overcome this limitation, Artal and Navarro[7] proposed a high-resolution imaging technique to obtain cone spacing information *in vivo*. That method was based on stellar speckle interferometry,[8] a technique commonly used in astronomy to resolve binary stars observed through ground-based telescopes, whose images are degraded by atmospheric turbulence. The standard method applied in astronomy consists of recording a large number of short-exposure images of the object and observing a point source through the same atmospheric turbulence. The recorded short-exposure images contain speckle patterns that are related to the structure of the object and carry diffraction-limited information. The average power spectrum of the speckle patterns is computed and is divided by the speckle transfer function (obtained as the average square modulus of the Fourier transform of the instantaneous point-spread function).

It has been shown that speckle interferometry can also be applied to obtain high-resolution information about objects observed through low-optical-quality telescopes[9] and about coherently illuminated objects.[10] In the case of the eye, aberrations are present in the optical system for large pupils,[11] and small areas of the fovea are illuminated with a (coherent) laser source. Although with this technique the phase information is lost and the object cannot be easily reconstructed, the average power spectrum gives important information about the structure of regular objects

0740-3232/96/050897-09$10.00

such as binary stars or the regular array of cones in the human fovea: Yellot[12] showed that the power spectrum of an excised fovea presented a roughly circular ring with a radius that was the inverse of the mean interdistance between rows of cones.

Williams *et al.*[13] recently proposed an imaging technique that uses spatially incoherent light, breaking the coherence of the laser source by means of two rotating diffusers. In that approach speckle patterns were not generated, but short-exposure images were taken to avoid blur produced by eye movements. Williams *et al.* also averaged the power spectra of individual short-exposure retinal images (as in the original idea of Artal and Navarro)[7] to increase the signal-to-noise ratio (SNR). Since they used incoherent light, the resolution of this fundus camera was limited mainly by the aberrations of the eye, although the researchers exploited the performance of the eye up to the limits imposed by the optics as they carefully compensated subjects' ametropia (defocus and astigmatism). Therefore with this method there were remote possibilities of resolving the cone mosaic in the foveal center,[14] where the cones are most densely packed. Williams *et al.*[13] looked for Yellot's rings at retinal eccentricities ranging from 0.25 to 2.5 deg. For these eccentricities it had been shown that the optical quality of the eye is as good as in the foveal center,[15,16] whereas the cone density shows an abrupt decline. They obtained results of cone interdistance that fitted well with the anatomical and psychophysical data.

In this paper we present a new system that we have developed on the basis of speckle interferometry to measure cone spacing in the living eye,[17] using coherent illumination, as was previously proposed by Artal and Navarro.[7] We show here that this method allows us to measure *in vivo* the characteristic spatial frequency of the cone mosaic in the range of retinal eccentricities tested with other objective techniques[13] and that the method makes it possible to resolve the cone mosaic in the foveal center.

2. METHODS

A. Apparatus

Figure 1 shows a diagram of the optical apparatus developed for the registration of short-exposure images of small patches of the retina. The light source is a green He–Ne laser (543 nm, 5 mW). The light passes through an electronic shutter (Uniblitz D122, Vincent Associates) that controls flash durations of 5 ms. The beam is focused by means of lens L_1 ($f = 60$ mm) onto a 200-μm pinhole (O), conjugate to the retina, that acts as a spatial filter. This pinhole is small enough to get a smooth and clean beam but is slightly bigger than the laser spot size. The area under test in the retina becomes illuminated by a Gaussian distribution of light. At the plane of the retina the beam intensity drops by the factor $1/e^2$ within a diameter of ~5 arcmin, which we consider to be the effective size of the illuminating spot. The beam is collimated by lens L_2 ($f = 60$ mm) before entering the eye. Since L_1 and L_2 have the same focal length, the beam is not expanded,[18] so that the entrance pupil of the system has a diameter of less than 1 mm. The advantage of this configuration is twofold: first, the light entering the eye is highly efficient, since it is not subject to the Stiles–Crawford effect, and scattering within the intraocular media is notably reduced; second, the depth of focus is large enough to allow the collimation of the beam not to be a critical factor. A pellicle beam splitter reflects 25% of the light toward the eye, while the transmitted light is absorbed by a light trap (LT). An artificial exit pupil (AP) is conjugate with the natural pupil of the eye, by means of lens L_3 ($f = 120$ mm). The light that is reflected back from the eye forms an aerial image one focal length from L_3. Then L_4 ($f = 120$ mm) and L_5 ($f = 500$ mm) cast the aerial image onto a CCD array. The CCD camera used in this experiment is a cooled, single-frame, scientific-grade CCD camera (SpectraSource, MCD1000) that contains a full-frame CCD array (Tektronix TK1024, 1.05 Mpixel). The format of the short-exposure images is 256×256 pixels with 16 bits/pixel. The pixel size is 24 μm on a side and subtends 0.16 arcmin with the described setup of lenses. The mechanical shutter within the CCD camera head is synchronized with the external electronic shutter, which is the one that determines the exact duration of the flash that illuminates the retina. The former opens an instant before the latter, which remains open for 5 ms. Then both shutters close. After the CCD exposure, the image is digitized and saved in a personal computer.

A second pellicle beam splitter allows the observer to view continuously, through the artificial pupil, an accommodation-fixation target, which is placed one focal length from L_6 ($f = 500$ mm) and thus is conjugate to the retina. The target consists of concentric circles crossed by perpendicular axes, printed on translu-

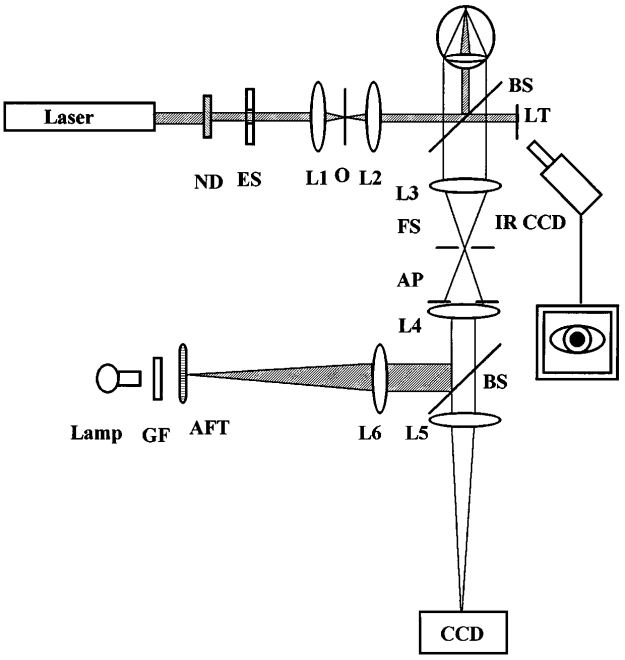

Fig. 1. Experimental setup. ND, neutral density filters; ES, electronic shutter; L_1, L_2, lenses (focal length = 60 mm); O, pinhole (diameter = 200 mm); BS, pellicle beam splitter; L_3, L_4, lenses (focal length = 120 mm); FS, field stop; AP, artificial pupil; L_5, L_6, lenses (focal length = 500 mm); CCD, high-resolution CCD camera; GF, green filter; AFT, accommodation-fixation target; LT, light trap; IR CCD, infrared CCD camera for monitoring the pupil size. The shaded areas indicate the ray path toward the eye. The ray tracing from the accommodation target has been partially omitted to avoid the overlapping with the beam reflected back from the eye.

cent diffuser paper. The intersections of the circles with the axes determine different retinal eccentricities (ranging from 0 to 1 deg) and locations (temporal, nasal, horizontal, and vertical) at which the observer fixates. Small letters printed on the target help the observers to keep their accommodations. The test is backilluminated with green light to eliminate changes in refraction that are due to longitudinal chromatic aberration. The accommodation-fixation target is aligned with respect to the beam so that its center is coincident with the laser spot.

Since, as will be described below, most of the experiments were performed with nondilated subjects, we inserted a subsystem to monitor the pupil of the nontested eye. Its size gives us an approximate value of the pupil size of the tested eye. If the natural pupil is smaller than the artificial pupil, it will be the effective exit pupil, and its diameter should be the one taken into account. The subsystem consists of an IR video camera that takes an image of the iris. This is displayed on a television monitor with a calibrated reticule attached.

B. Observers

Measurements were made on five observers: MA, MR, PA, RN, and SM, with ages ranging from 24 to 37 years (32 on average) and with different amounts of refractive error, myopias ranging from -0.5 D to -7 D. Two observers, MA and RN, also needed compensation for astigmatism, -0.75 D and -0.5 D, respectively. These ametropias were corrected during the experiment, as described below, and when the subjects kept their natural accommodations, they included the instrumental myopia. All of the observers used the right eye, except for MR, who used his left eye.

Most of the measurements were performed under natural viewing conditions and with pupil diameters of $\sim$5 mm. Control experiments and the measurements in the center of the fovea were carried out on three observers with their pupils dilated.

C. Experimental Procedure

The observer's head was stabilized by means of a bite bar, mounted on a three-dimensional micropositioner. The alignment was achieved by geometrically centering the subject's pupil with respect to the laser beam, conveniently attenuated for this purpose. For this centered position, the fixation target was also seen with maximum contrast.

The refractive correction was subjectively determined, by means of trial lenses, using the letters of the accommodation-fixation target as a refraction chart. The intensity of the light that illuminated the target was adjusted to the observer's preference. This was the main factor that determined the natural pupil size. After these settings, and right before the image acquisition, the laser beam was blocked and some neutral density filters were removed. The total power incident upon the cornea was 30 μW. This irradiance was 2.35 orders of magnitude below the ANSI Z-136.1 maximum permissible limit for a 5-ms exposure.[19]

The observers were requested to fixate to a specific intersection on the target and to maintain their accommodation during the exposure. The pupil size was controlled at different moments during the course of the experiment. All of the observers found that the flashes were comfortable enough and that the task of fixating and accommodating was quite easy, and they appreciated the rapidity of the procedure.

In contrast to the several hundreds of frames typically recorded in astronomical applications, we registered a series of only 12–24 short-exposure images for each retinal location. There were two main reasons for this: first, in astronomy the amount of light is usually limited to a few photons per frame; in our case we used a bright laser beam so that each frame contained a large number of photons; thus it was not necessary to record so many frames to increase the SNR. Second, we performed experiments in humans, and the observer's comfort was considered a priority. After the acquisition of the series, a bias field on the CCD array was collected.

Retinal eccentricities outside the center of the fovea (0.25, 0.5, and 1 deg) were tested at various azimuths for most of the observers under natural vision conditions. Experiments were carried out in the center of fovea with the pupil dilated and the accommodation paralyzed with cyclopentolate 1%, two drops, administered one drop at a time, 5 min apart. Some control experiments were also performed with other mydriatics (tropicamide 1% and hydroxyamphetamine-hydrobromide 1%-tropicamide 1%).

D. Image Processing

The images were digitally processed after acquisition. First, the bias field was subtracted from all the images. Then the power spectrum—the square modulus of the fast-Fourier transform—of each image of the series was computed. In order to enhance the higher frequencies, we represented the power spectra in a logarithmic scale, and the central pixels, much brighter than the rest of the image, were not displayed.

A selection of good individual images, with respect to the speckle pattern as well as to the power spectrum, helps to improve the results considerably, in the sense of finding a ring or signal in the average power spectrum. Rings (or hexagons) were clearly visible in some single power spectra, in spite of the speckle noise, indicating that the amount of light per frame was high enough to produce individual power spectra with a good signal. Figure 2(a) shows a typical series of speckle patterns recorded in the laboratory, and Fig. 2(b) shows the corresponding power spectrum for each single image. This particular series corresponds to subject MA, at an eccentricity of 0.5 deg inferior. All the images are represented on an arbitrary linear scale, with their intensities normalized to the respective peaks. The recorded short-exposure images had maximum intensities of $\sim$12 bits (15% of the maximum possible value). Several images were rejected for various reasons: image 4 was blurred, probably because of an eye movement, which produced a power spectrum with low resolution; speckles in image 8 were spread over a larger area than in the rest of images, indicating a change in the accommodative state that produced a defocus; only two bright speckle grains were present in image 10, producing a power spectrum with bright fringes, which mask the higher-frequency content; possibly as a result of a fixation error, image 11 corresponds to a higher retinal eccentricity, which is obvious in the power spectrum that

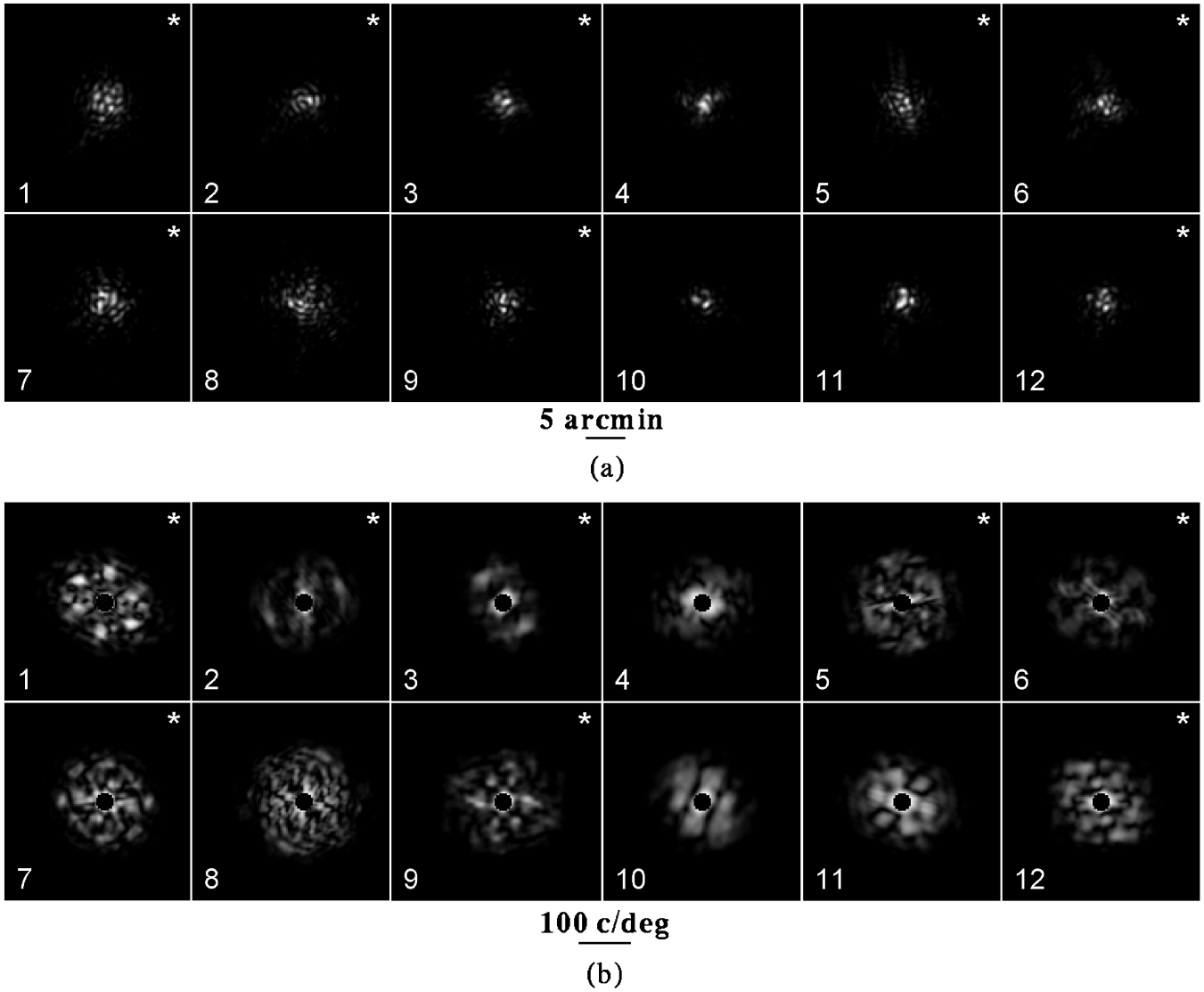

Fig. 2. (a) Series of 12 short-exposure images, corresponding to subject MA, at 0.5 deg of retinal eccentricity, inferior. The images marked with an asterisk at the upper-right corner were selected as the best speckle patterns, and the four remaining ones were rejected, according to the reasons explained in the text. (b) Power spectra of each of the images shown in (a). They are represented in a logarithmic scale, and the central peak has been removed.

presents a regular structure at a lower frequency than others in the series. Therefore four of the twelve images of this particular series were rejected. The rest of the speckle patterns are quite good. They show in many cases a regular structure correlated with that of the foveal mosaic, and their corresponding power spectra present a more or less evident hexagon (which is expected from a perfectly regular array) or ring (if the principal axes of the array are not perfectly defined) of the same appearance. The average ratio of acceptably good images was approximately 40%. For some cooperative and particularly trained observers, the ratio was higher, in certain cases up to 100%.

The power spectra of the selected images were averaged and processed for display as described above.

3. EXPERIMENTAL RESULTS

The recorded short-exposure images show in many cases a nonrandom speckle pattern. Under favorable circumstances a regular packing of the speckle grains, which recalls the hexagonal structure of the foveal mosaic, appears in the images. See, for example, image 1 in Fig. 2(a). For these specific cases a clear hexagon appears even in the power spectrum corresponding to an individual image. Nevertheless, speckle patterns with no regular structure and no periodic component in the power spectra had been observed in control experiments that used an artificial eye, which consisted of a lens and a perfect diffuser in place of the retina.

Most of the computed average power spectra show an evident ellipse, ring, or hexagon of different radius for each observer and/or eccentricity. We analyzed the gray-level images to extract the parameters of the rings, which gave us information about the packing of the foveal cones. When the ring was elliptical, the principal axes of the ellipse, as well as its orientation, were identified. The sections along the axes presented clear peaks at the location of the ring, which provided the upper and lower values of the characteristic spatial frequencies of the cone mo-

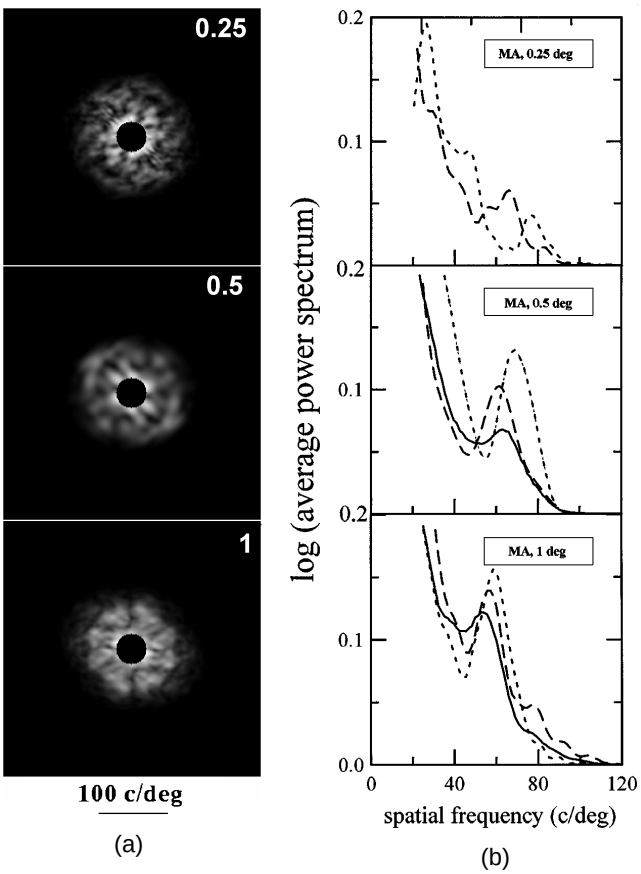

Fig. 3. (a) Two-dimensional average power spectra, for subject MA for 0.25, 0.5, and 1 deg of retinal eccentricities, processed as described in the text. (b) One-dimensional representations of the average power spectra shown in (a): sections along the minor (long-dashed curves) and major (short-dashed curves) axes of the elliptical ring, and radial profile when it is significant (solid curves).

saic. In general, if the ring was roughly circular, a distinct bump appeared when averaging was done over all directions (radial profile). This value lay between the ones obtained through the sections along the axis but was not always the exact arithmetical mean. Sometimes the radial profile was too flat, or the bump too broad, to extract from it any reliable data. The final characteristic spatial frequency of the mosaic for a given eccentricity assigned to each subject was computed, in general, as the mean of the spatial frequencies obtained from the principal axes.

Figure 3(a) shows the logarithm of the average power spectra for observer MA for three retinal eccentricities (0.25, 0.5, and 1 deg), inferior. The rings appearing at 0.25 and 0.5 deg of eccentricity are slightly elliptical (ratio of the axes, 1.17 and 1.13, respectively), whereas a hexagon appears at 1 deg. It can be observed that other more complex structures are also present at lower spatial frequencies. Figure 3(b) shows one-dimensional plots of these power spectra. Long-dashed and short-dashed curves represent sections along the minor and the major axis, respectively, and the solid curves represent the radial profile. In all of the cases, except for the radial profile corresponding to 0.25 deg of retinal eccentricity, very sharp peaks reveal the characteristic spatial frequencies of the mosaic. As a consequence of the presence of other structures at lower spatial frequencies with a less defined geometry, other peaks of lower contrast are present in some of the sections plotted in these graphs.

The decline in the characteristic spatial frequency as a function of the eccentricity is clear for this subject. The cone spacing values, as well as the ellipticity of the ring or its orientation, vary notably between subjects, as can be observed in Fig. 4, which represents the average power spectra for three other subjects (RN, SM, and PA) at 0.5 and 1 deg of retinal eccentricity. Nevertheless, the tendency pointed out above is common for all the subjects.

We also obtained rings in the power spectra for two subjects (MA and RN) of the four who were tested in the center of the fovea. Bumps in the radial profile reveal the characteristic spatial frequency of the mosaic in the foveal center as the mean radius of these rings.

The variation of the spatial frequency of the cone mosaic for all the subjects is summarized in Fig. 5 as a func-

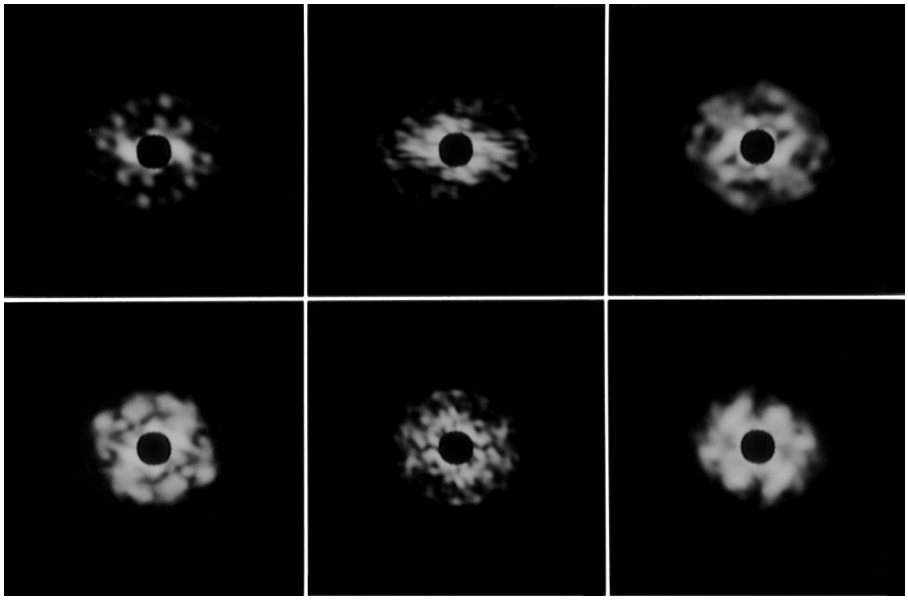

Fig. 4. Two-dimensional average power spectra, processed as described in the text, for three subjects: RN (left), SM (middle), and PA (left), and two different retinal eccentricities: 0.5 deg (top) and 1 deg (bottom).

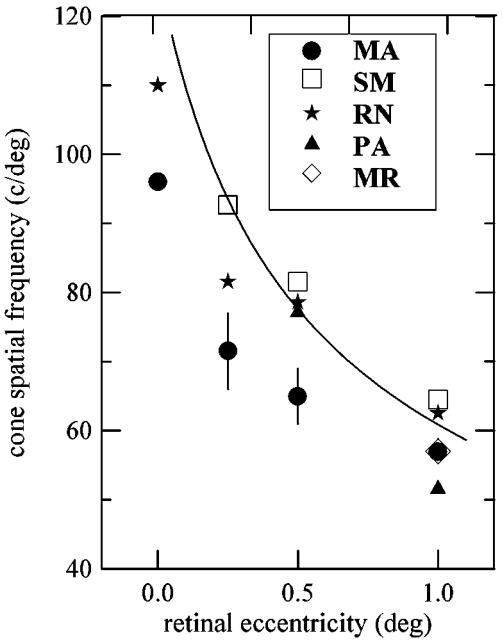

Fig. 5. Spatial frequency of the cone mosaic (mean radius of the rings in the average power spectra) as a function of the retinal eccentricity for various subjects. The length of the bars, plotted only for subject MA, indicate the range of spatial frequencies covered between the principal half-axes of elliptical rings. The solid curve represents a fit of the average histological data.

tion of retinal eccentricity. Each subject is identified by a different symbol. The symbols represent the characteristic spatial frequency of the cone mosaic, obtained as the average of the half-axes of the elliptical ring. The length of the bars centered on the symbols (which, for the sake of clarity, have been plotted only for subject MA) represent the range of frequencies covered between the half-axes. The solid curve represents an analytic fit[20] of the spatial frequency of the cone mosaic as a function of retinal eccentricity, derived from the average anatomical data for cone densities of Curcio *et al.*[2], assuming hexagonal packing, and from the conversion factor[3] of 280 μm/deg: $f = 126.58/\sqrt{(1 + 3.32\epsilon)}$, where f is the spatial frequency of the cone mosaic in cycles per degree (c/deg) and ϵ is retinal eccentricity in degrees.

For all subjects there is a clear decrease in the characteristic spatial frequency of the cone mosaic with retinal eccentricity. For each subject the curves have different slopes, in agreement with a similar tendency of the anatomical data.

4. DISCUSSION

The results on the foveal topography obtained with the speckle interferometry technique, at retinal eccentricities from 0 to 1 deg, range from 110 to 52 c/deg. These values are consistent with the anatomical data[2] as well as with the psychophysical data,[4] and with recent objective results.[13]

Our *in vivo* imaging technique, as well as the incoherent method by Williams *et al.*,[13] has proved to be successful in obtaining the characteristic spatial frequency of the cone mosaic at retinal eccentricities close to the foveal center. Furthermore, we have also been able to resolve the cone spacing in the center of the fovea. In both methods, short-exposure images are recorded. As a consequence, blurring of the cones or the speckle patterns, produced by eye movements, is avoided. Since Williams *et al.* used incoherent imaging, they stated that the potential resolution should be limited by the aberrations of the eye, so that the cutoff frequency of the incoherent modulation transfer function imposes an upper bound to the frequencies that can be resolved. If the cone mosaic needs to be resolved in the center of the fovea, spatial frequencies of 120 c/deg and higher must be allowed to pass through the optics of the eye. In diffraction-limited optical systems, it is possible to achieve this by increasing the exit-pupil aperture. Nevertheless, if aberrations are the most important source of degradation of the images, there is no point in increasing the pupil size to gain resolution, since it is well known that the performance of the optical system of the eye deteriorates with large pupils.[11] Thus, unless the wave-front aberration is corrected[21] and the effects of aberrations are reduced when large pupils are used, it would be fairly impossible, with incoherent light, to resolve the cones at 0 deg of retinal eccentricity.

When coherent light is used, the speckle patterns in principle carry information up to the diffraction limit of the optical system. The effect of aberrations is to reduce the SNR, but in any case the cutoff frequency of the power spectra goes up to the diffraction limit.[10] We performed experiments on three subjects (SM, PA, and MR) with their pupils dilated, to estimate the resolution for different pupil sizes. Figure 6 shows an example of typical short-exposure images for subject MR obtained through artificial pupils of diameters of 2, 5, and 8 mm. Figure 7 summarizes the results of this experiment for three observers. The straight (solid) line represents the cutoff spatial frequency of the diffraction-limited system as a function of pupil size and for a wavelength of

Fig. 6. Short-exposure images for different pupil diameters: 2 mm (left), 5 mm (middle), and 8 mm (right), corresponding to observer MR at a retinal eccentricity of 1 deg. The speckle grains become smaller with increasing pupil size.

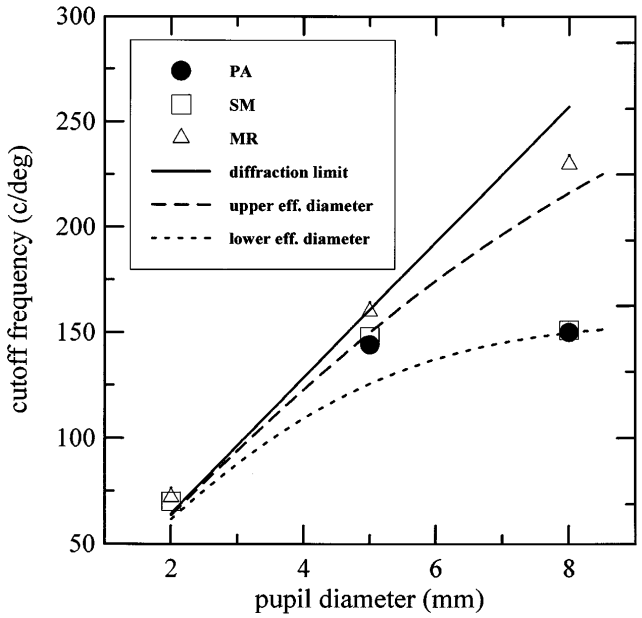

Fig. 7. Resolution (cutoff spatial frequency of the average power spectra) as a function of pupil diameter for three subjects. The solid line represents the resolution of a diffraction-limited system at a wavelength of 543 nm as a function of the apparent pupil diameter. The curves also represent the resolution of a diffraction-limited system but for the effective pupil size, taking into account the Stiles–Crawford effect. Long-dashed curve, $\rho = 0.02$; short-dashed curve, $\rho = 0.075$.

543 nm. The symbols represent the cutoff frequencies of the average power spectra for the three subjects; each cutoff is computed as the spatial frequency beyond which SNR < 1. The noise level is estimated as the mean intensity level beyond the theoretical cutoff spatial frequency, assuming white noise. All of the subjects almost reached the diffraction limit at the smaller pupil sizes, but for an 8-mm pupil a discrepancy of more than 150 c/deg appeared for subjects SM and PA. In contrast, the cutoff frequency for subject MR for an 8-mm pupil (230 c/deg) remained very close to that of the perfect system (257 c/deg). There could be a straightforward explanation for the especially high resolution found in MR in comparison with that of the other two observers, who stayed far from the theoretical limit. Subject MR is known to exhibit a relative flat Stiles–Crawford effect,[22] which means that the effective pupil is close to its physical size. It has been shown that many optical parameters related to pupil size (for example, depth of field or lateral chromatic aberration) differ from the expected value and that such deviation from theoretical expectation can be accounted for by the operation of the Stiles–Crawford apodization.[23] Let us consider the curve of the Stiles–Crawford effect: $\eta = \eta_{\max} 10^{-\rho(x-x_{\max})^2}$, where η is the brightness sensitivity in relative units, ρ gives the flatness of the Stiles–Crawford effect, and $(x - x_{\max})$ is the distance in the pupil plane (in millimeters) from the location of the peak of sensitivity ($\eta_{\max}$). The effective pupil size, which is defined as the pupil size that would give rise to a given subjective brightness if there were no retinal effect, can be calculated from any apparent pupil size: $d_e = \sqrt{[1 - \exp(-0.575\rho d^2)]/2.30\rho}$, (where d_e and d are the effective and the apparent pupil diameters, respectively). We derived the effective pupil diameter as a function of the known rho value ($\rho = 0.02$)[19] in MR's Stiles–Crawford-effect curve and represented the theoretical diffraction limit as a function of the effective pupil diameter (long-dashed and short-dashed curves) instead of the apparent pupil diameter (solid line). Applegate and Lakshminarayanan[24] found, for a group of 54 observers, rho values ranging from 0.02 to 0.075. Thus MR would represent the case of an upper limit for effective pupil size. The short-dashed curve represents the diffraction limit corresponding to an apparent pupil size for a rho value of 0.075. The values for the other two observers (PA and SM) lie closer to this lower limit, corresponding to a rho value of 0.075. Further research is planned on that point. Other definitions of effective pupil size could be considered. In addition, the relationship between the rho values of the curves obtained from psychophysical methods and from objective measurements of the fundus reflectance (as in our case) is not yet well established.[25] The resolution for large pupils achieved with our method seems, therefore, to depend on the subject. Natural-pupil sizes of ~5 mm give, in general a resolution close to 150 c/deg and can be moderately (SM, PA) or extremely (MR) improved by dilating the pupil. The most recent histological data showed characteristic spatial frequencies ranging from 95 to 169 c/deg for a group of eight eyes. Consequently, for many observers, especially for those without very densely packed cones or with a wide effective pupil, it will be possible to resolve the cones in the foveal center. We obtained results in the center of the fovea in subjects MA and RN, with characteristic spatial frequencies of 95 and 110 c/deg, respectively. Nevertheless, no evidence for a ring was obtained for subject MR, who had the highest resolution in the power spectra.

The fact that the resolution depends on the effective pupil size supports the idea that most of the collected light is reflected back from the photoreceptors. The scattered light present in the images seems to be minimized when green light is used.[26] Average power spectra, corresponding to a series of images registered with use of a red laser beam, reach cutoff frequencies closer to the diffraction limit but do not show any ring revealing the cone array.

Figure 8 compares the range covered by our results with the range obtained by Williams *et al.*[13] After averaging all the subjects, our data are lower by 16% on average, with the greatest difference for 0.25 deg. It is likely that the cause of most of this difference is intersubject variability, since the populations in the two studies were different. For a given eccentricity, the range of frequencies covered by all the subjects under study is very broad, the closer the eccentricity to the central fovea, the larger the range. For example, at 0.5 deg of retinal eccentricity, cone spatial frequencies for eight eyes studied by Curcio *et al.*[2] covered a range of spatial frequencies of 43 c/deg. At the same eccentricity, Williams *et al.*[13] reported a range of 16 c/deg, comparable to ours of 20 c/deg. We carried out a direct comparison of the two techniques on observer RN. He had been tested 10 months before, at the same retinal locations, with the apparatus developed at the University of Rochester.[13] For this observer, at 0.5 deg of eccentricity, we found a difference of 6.3 c/deg

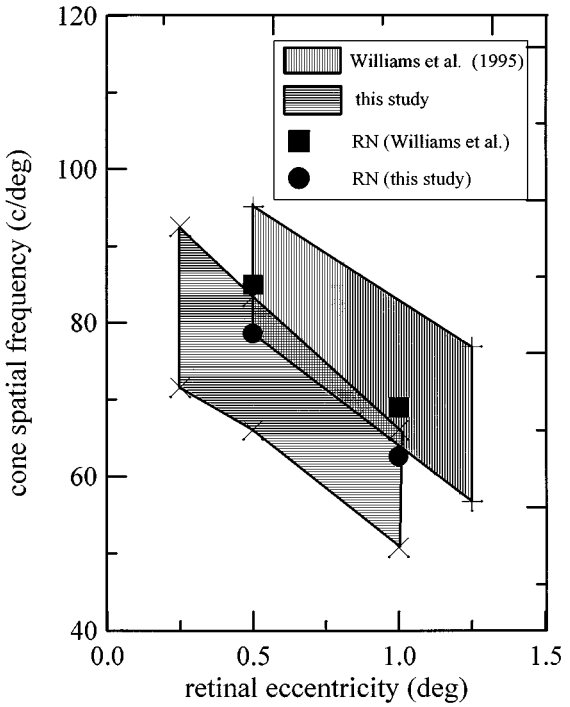

Fig. 8. Comparison between the range of spatial frequencies of the cone mosaic obtained by Williams *et al.*[13] and from the measurements that we present here.

(our result was only 7.5% lower), and at 1 deg of eccentricity, 6.4 c/deg (9.3% lower). The small discrepancies can be explained by the fact that we collected data from a very small area in the fovea. Thus any small change in fixation will give slightly different results because of the rapid change in cone spacing with eccentricity. In fact, the indetermination of the measurement, as defined by the half-width of the bumps in the one-dimensional plots (12 c/deg on average), is higher than the discrepancy. Another point that we should bear in mind in this respect is that our average power spectra are in fact affected by a speckle transfer function. As we mentioned above, in astronomical applications the object power spectrum is recovered by dividing by the speckle transfer function, usually obtained by averaging the squared modulus of the fast-Fourier transform of short-exposure images of a point registered through the same aberrating media. It is not possible to measure the exact form of this function in our case. As a result, the peaks appearing in our power spectra may be a little shifted toward lower frequencies, and thus the measured radius of the Yellot's ring may be slightly underestimated. We have derived a simple computer simulation model that yields a decrease of ~8%, which would explain the average discrepancies observed with respect to other methods.

We have found some evidence of anisotropy in cone spacing, which is in agreement with anatomical and psychophysical data. The aspect ratio of the elliptical rings appearing in the power spectra ranges from 1 to 1.32. With averaging across all the subjects and eccentricities tested, the average aspect ratio is 1.15. Williams, with his psychophysical techniques,[4] observed for one subject at 0.75 deg of retinal eccentricity that the horizontal separation between cones was 1.16 times larger than the vertical separation. For three other observers he also found a tendency for the spacing between cones to be slightly greater in the horizontal direction than in the vertical direction at any retinal location in the fovea. With our technique this would yield an ellipse in the power spectrum with its major axis along the vertical direction. We have not detected a clear tendency toward a specific orientation of the ellipse in our subjects. The aspect ratio of the ellipse and its tilt vary slightly from one eccentricity to the next within the same subject and significantly among different subjects. This was to be expected, since we obtained our data by recording very small patches of the retina, with only a few cones, and the orientation of the principal axes of the mosaic could randomly change from one location to another. Slight changes in the orientation and eccentricity of the ellipse were observed when we repeated the measurements for one observer under the same conditions. Computational simulations of the power spectrum of digitized images of the cone mosaic in excised retinas from the study by Curcio *et al.*[2] also showed ellipses with no particular orientation and ellipticity. It is worth noting that for 1 deg of eccentricity we found clear hexagons in the average power spectra in three (MA, RN, and PA) of the five subjects tested. The explanation of this fact is not that cones are more regularly packed at this eccentricity but that fewer cones are illuminated at a time, and thus fewer changes in the orientation of the principal axes of the hexagonal array are possible.

No attempt was made in the present study to perform a detailed analysis of the anisotropy in the topography of the cone mosaic along meridians. In fact, the results presented here correspond to different meridians: inferior for subjects MA and SM, superior for RN, temporal for PA, and nasal for MR. Apparently, the meridional anisotropy is not strongly evident at the range of eccentricities that we are considering.[4]

In summary, we have developed a new apparatus to determine, *in vivo*, the local cone packing in the human fovea, on the basis of the speckle interferometry method by Artal and Navarro.[7] We have obtained repeated successful results at eccentricities ranging from 0.25 to 1 deg as well as the first objective data of cone spacing at the center of the fovea *in vivo*, for two observers. Additional experiments and further research on the limits of the method will allow us to perform measurements in the foveal center on a regular basis in a large number of observers.

ACKNOWLEDGMENTS

This research has been supported by the Comisión Interministerial de Ciencia y Tecnología (Spain) under grant TIC94-0849. We thank subjects M. Angeles Losada and Maurice Rynders for their kind collaboration. We are also grateful to David Williams, Don Miller, Ann Elsner, Steve Burns, and Dan Green for helpful discussions.

REFERENCES

1. G. Osterberg, "Topography of the layer of rods and cones in the human retina," Acta Ophthalmol. Suppl. **6,** 1–97 (1935).
2. C. A. Curcio, K. R. Sloan, R. E. Kalina, and A. E. Hendrickson, "Human photoreceptor topography," J. Comp. Neurol. **292,** 497–523 (1992).

3. N. D. Drasdo and C. W. Fowler, "Non-linear projection of a retinal image in a wide-angle schematic eye," Br. J. Ophthalmol. **58,** 709–714 (1974).
4. D. R. Williams, "Topography of the foveal cone mosaic in the living human eye," Vision Res. **28,** 433–454 (1988).
5. W. S. Jagger, "Visibility of photoreceptors in the intact living cane toad eye," Vision Res. **25,** 729–731 (1985).
6. M. F. Land and W. A. Snyder, "Cone mosaic observed directly through the natural pupil of live vertebrate," Vision Res. **25,** 1519–1523 (1985).
7. P. Artal and R. Navarro, "High-resolution imaging of the living human fovea: measurement of the intercenter cone distance by speckle interferometry," Opt. Lett. **14,** 1098–1100 (1989).
8. J. C. Dainty, ed. *Laser Speckle and Related Phenomena* (Springer-Verlag, Berlin, 1984), Chap. 7, pp. 255–320.
9. J. C. Dainty, "Diffraction-limited imaging of stellar objects using telescopes of low optical quality," Opt. Commun. **5,** 129–134 (1972).
10. T. Mavroidis, J. C. Dainty, and M. J. Northcott, "Imaging of coherently illuminated objects through turbulence," J. Opt. Soc. Am. **7,** 348–355 (1990).
11. P. Artal and R. Navarro, "Monochromatic modulation transfer function of the human eye for different pupil diameters: an analytical expression," J. Opt. Soc. Am. A **11,** 246–249 (1994).
12. J. J. Yellot, "Spectral analysis of spatial sampling of photoreceptors: topological disorder prevents aliasing," Vision Res. **22,** 1205–1210 (1982).
13. D. R. Williams, D. Miller, and G. M. Morris, "Images of the cone mosaic in the living human eye," in *Vision Science and Its Applications*, Vol. 1 of 1995 OSA Technical Digest Series (Optical Society of America, Washington D.C., 1995), pp. 98–101.
14. M. R. Atkinson, A. Roorda, and M. C. W. Campbell, "Imaging of individual photoreceptors beyond the incoherent resolution limit," Invest. Ophthalmol. Vis. Sci. Suppl. **35,** S188 (1995).
15. P. Artal and R. Navarro, "Simultaneous measurement of two point-spread functions at different locations across the human fovea," Appl. Opt. **31,** 3646–3656 (1992).
16. R. Navarro, P. Artal, and D. R. Williams, "Modulation transfer of the human eye as a function of retinal eccentricity," J. Opt. Soc. Am. A **10,** 201–212 (1993).
17. S. Marcos, R. Navarro, and P. Artal, "Foveal cone mosaic imaged *in vivo* by an objective high-resolution imaging technique," in *Lasers in Ophthalmology III*, R. Birngruber and A. S. Fircher, eds. Proc. SPIE **2632,** 48–55 (1995).
18. R. Navarro and M. A. Losada, "Phase transfer and point-spread function of the human eye determined by a new asymmetric double-pass method," J. Opt. Soc. Am. **11,** 2385–2392 (1995).
19. D. Sliney and M. Wolbarsht, *Safety with Lasers and Other Optical Sources* (Plenum, New York, 1980).
20. A. Tabernero, "Representación de imágenes mediante funciones de Gabor. Modelado del sistema visual y análisis de texturas," Ph.D. dissertation (Universidad Complutense de Madrid, Madrid, 1992).
21. A. W. Dreher, J. F. Bille, and R. N. Weinreb, "Active optical depth resolution improvement of the laser tomographic scanner," Appl. Opt. **4,** 804–808 (1989).
22. M. C. Rynders, "The Stiles–Crawford effect and an experimental determination of its impact on vision," Ph.D. dissertation (Indiana University, Bloomington, Ind., 1994).
23. F. W. Campbell, "The depth of field of the human eye," Opt. Acta **4,** 157–164 (1957).
24. R. A. Applegate and V. Lakshminarayanan, "Parametric representation of Stiles–Crawford functions: normal variation of peak location and directionality," J. Opt. Soc. Am. A **10,** 1611–1623 (1993).
25. S. A. Burns, S. Wu, F. Delori, and A. E. Elsner, "Direct measurement of the human-cone-photoreceptor alignment," J. Opt. Soc. Am. A **12,** 2329–2338 (1995).
26. D. R. Williams, D. H. Brainard, M. J. McMahon, and R. Navarro, "Double-pass and interferometric measures of the optical quality of the eye," J. Opt. Soc. Am. A **11,** 3123–3135 (1994).